


Application of UAV, GNSS and InSAR Techniques in the Raw Material Supply Chain

Tanja Grabrijan¹ ^a, Kristof Oštir¹, Klemen Kozmus Trajkovski¹, Dejan Grigillo¹, Veronika Grabrovec Horvat¹, Polona Pavlovčič Prešeren¹, Veton Hamza¹, Antonio Pepe², Fabiana Calò², Francesco Falabella², Enoc Sanz-Ablanedo³, Mihaela Gheorghe⁴, Teodora Selea⁴ and Ana Cláudia Teodoro⁵

¹University of Ljubljana, Faculty of Civil and Geodetic Engineering, Jamova cesta 2, Ljubljana, Slovenia

²Italian National Research Council, Institute for Electromagnetic Sensing of the Environment (IREA), 328, Diocleziano, Napoli, Italy

³Grupo de Investigación en Geomática e Ingeniería Cartográfica (GEOINCA), Universidad de León, León, Spain

⁴GMV Innovating Solutions SRL, Bucharest, Romania

⁵University of Porto, Department of Geosciences, Environment and Spatial Planning, and Institute of Earth Sciences (ICT), Rua do Campo Alegre 687, Porto, Portugal

{tanja.grabrijan, kristof.ostir, klemen.kozmus-trajkovski, dejan.grigillo, veronika.grabrovec-horvat,

Keywords: Mining, UAV, Tri Stereo, SfM Photogrammetry, Low-Cost GNSS, InSAR, Super-Resolution.


Abstract: The marble quarry, located in southern Austria produces high-quality marble, both in open-pit and underground extraction sites. Extraction, transportation and accumulation of material require close monitoring to maintain the stability of the whole area and to observe changes in waste dumps. In this study, we have shown how different methodologies can be used to support the monitoring of the entire raw material supply chain. Several unmanned aerial vehicle (UAV) surveys were performed to compute high-resolution digital elevation models (DEM) to serve as a reference for comparing stereo and tri-stereo DEMs calculated from satellite imagery. A low-cost global navigation satellite system (GNSS)-based monitoring system was set up to estimate horizontal and vertical displacements. In addition, the state-of-the-art technique of Interferometric synthetic aperture radar (InSAR) provided displacement time series for a broader area.

1 INTRODUCTION

The Secure and Sustainable Supply of Raw Materials for EU Industry (S34I) project aims to increase European autonomy over raw materials resources through research and development of new data-driven methods for analysing Earth observation (EO) data. It will improve the systematic exploration of minerals and ensure continuous monitoring of all mining activities, i.e., extraction, closure, and post-closure.

This paper presents the preliminary results using various techniques and methods, including satellite data, airborne systems, unmanned aerial vehicles (UAVs), ground-based measurements, and traditional in-situ methods. Improved volume maps of mining

waste deposits using a multispectral sensor mounted on a UAV have been used at the extraction site. Ground instability maps are obtained through new InSAR methods for the Sentinel-1 radar data to compute long-term, i.e. 2014-2023 ground displacement time series. Mineral stockpile volume is calculated through satellite photogrammetry from optical data. Displacement time series are measured and analysed using low-cost global navigation satellite system (GNSS) receivers. The results presented are preliminary and will require further validation to ensure their accuracy and reliability for long-term monitoring applications.

^a <https://orcid.org/0009-0009-7374-9251>

2 STUDY AREA

The extraction site is located in southern Austria and produces high-quality marble, both in open-pit and underground extraction sites. This marble formed during the Devonian period, around 350-400 million years ago, and has a colour ranging from light grey to white. This material is used to produce mineral fillers and pigments. In this study, only the open pit mine is considered. The slopes are represented by hard rock, which requires high-precision measurements to assess their stability. The area of interest is about 1.2 km² and includes a waste dump and an active quarry (Figure 1).

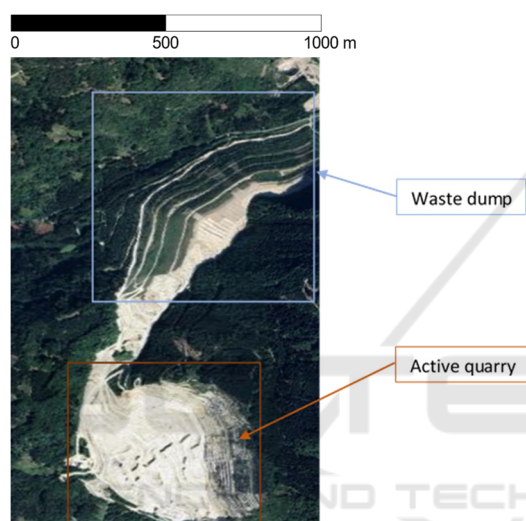


Figure 1: The area of interest: waste dump and active quarry.

3 InSAR DISPLACEMENT MAPPING

Multi-frequency and multi-orbit SAR satellite data were used for Interferometric SAR (InSAR) displacement mapping purposes. C-Band Sentinel-1 A/B ascending and descending complex SAR images gathered from October 2014 to March 2023 were used. Complementary to medium-resolution Sentinel-1 images, high-resolution X-Band COSMO-SkyMed SAR images acquired along the descending orbit were also used.

Sentinel-1 images were independently processed by following the standard steps of SAR image registration, topography removal using an external one arc-second Shuttle Radar Topography Mission (SRTM) Digital Elevation Model (DEM), orbit compensation via precise Sentinel-1 supplementary

information, additional fine co-registration procedure on the images, and finally, interferograms generation. The interferograms were then unwrapped using the multigrad algorithm (Falabella et al., 2022) to obtain the high-resolution unwrapped phases. Line-of-sight (LOS)-projected ground displacement time series were obtained by inverting the unwrapped single-look interferograms via Small Baseline Subset (SBAS) algorithm (Berardino et al., 2002).

The same processing operations, up to the unwrapping stage, were also performed on COSMO-SkyMed datasets. Subsequently computed Sentinel-1 vertical (up-down) and horizontal (east-west) ground displacement time-series were used in feedback to the multigrad unwrapping operation for flattening the COSMO-SkyMed interferograms. This auxiliary step was incorporated into the processing flow to facilitate phase-unwrapping by reducing low-frequency displacement contributions, thereby minimizing ambiguity numbers during the unwrapping process. Once they were unwrapped, the COSMO-SkyMed LOS displacements were obtained, as well as the enhanced combined Sentinel-1 (resampled onto the spatial resolution grid of COSMO-SkyMed) and COSMO-SkyMed vertical (up-down) and horizontal (east-west) displacement time-series.

The multisensor data combination aims to enhance the temporal sampling of measurements rather than perform cross-calibration. Independent ground displacement time-series are computed and geocoded before solving a constrained linear problem to derive 2-D ground displacement time-series, following Pepe et al. (2016).

Results are shown in Figure 2 and Figure 3. Figure 2 shows the 2-D InSAR products obtained using the detailed multigrad InSAR methodology, while Figure 3 shows displacement time-series related to the SAR measure point indicated in Figure 2.

4 DEEP LEARNING FOR SAR IMAGE ENHANCEMENT

We investigated several deep learning models using Sentinel-1, Sentinel-2 and COSMO-SkyMed (CSK) data to improve the resolution of Synthetic Aperture Radar (SAR) images. The dataset used in this study comprises 135,013 patches extracted these images. The CSK data preprocessing involved using a half-band filter to generate the corresponding low-resolution (LR) images for training purposes. This filter applies downsampling while preserving phase information, which is essential for SAR applications

**IREA-CNR (Multigrid InSAR Processing)
2-D (Vertical and Horizontal) InSAR Ground Displacement Profiles**

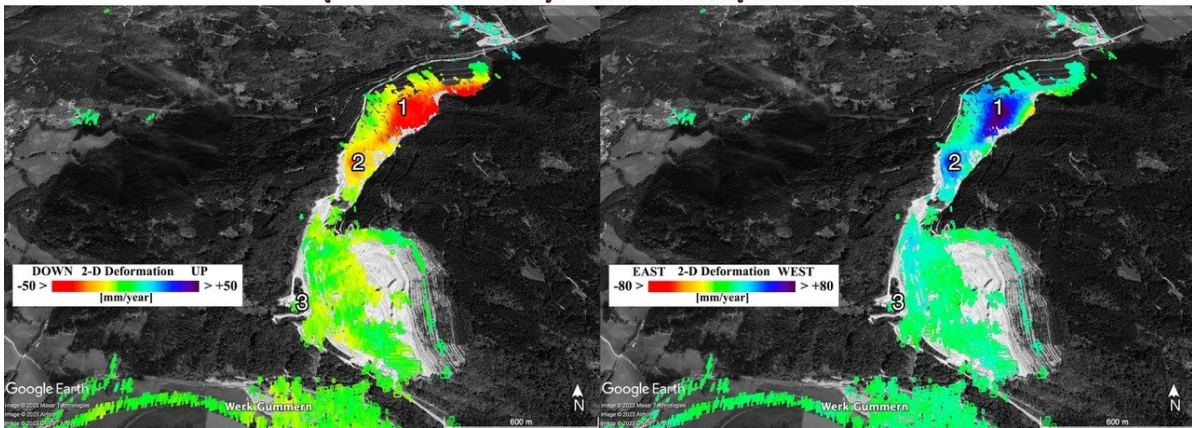


Figure 2: Deformation velocity maps generated through advanced InSAR processing technique show vertical (left) and horizontal (right) components of displacements.

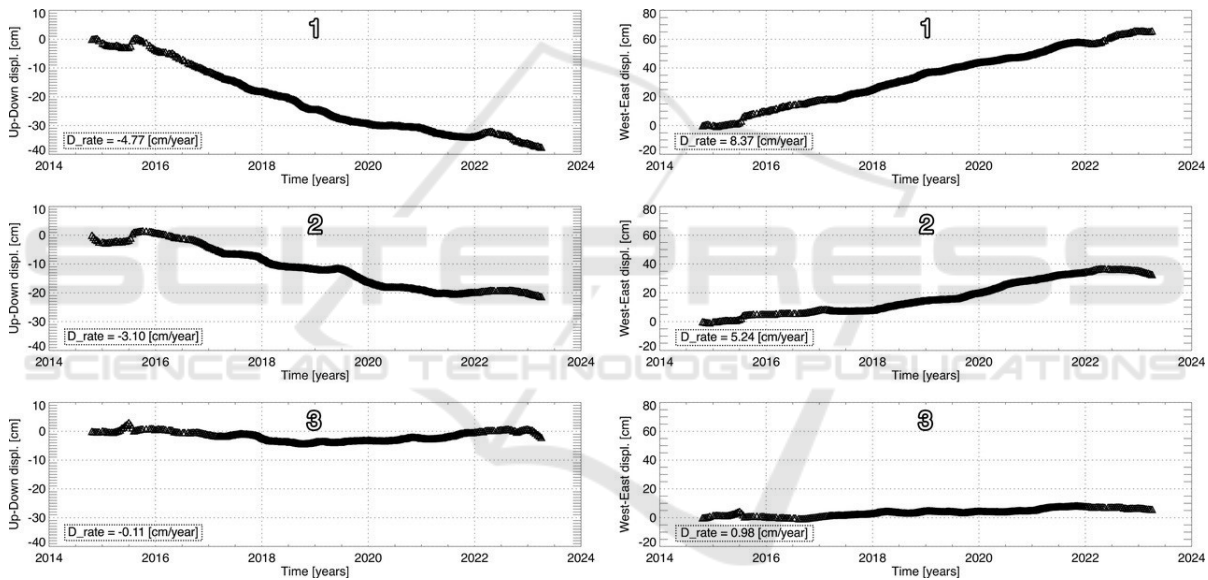


Figure 3: Displacement time-series related for points indicated in the upper map. From the top: first two time series show the subsidence (Up-Down) and Horizontal (E-W) deformation trend. At the bottom: time series related to stable measurement points. Also, the velocity of deformation is reported in the graphs.

such as interferometry. Each SAR CSK patch consists of real and imaginary components, and the filter was applied independently to each channel. Sentinel-1 patches from the Sen1-2 dataset, and its optical Sentinel-2 equivalents acted as supplementary inputs in several models.

We evaluated the following deep learning architectures for SAR super-resolution:

1. Residual-in-Residual Dense Block (RRDB) (Wang et al., 2018): A convolutional neural network that incorporates multiple residual

blocks to enhance feature extraction and avoid information loss.

2. Super-Resolution U-Net (SRUN) (Ronneberger et al., 2015): A modified U-Net architecture optimized for SAR data, integrating downsampling and upsampling layers for effective feature recovery.
3. Optical-Guided Super-Resolution Network (OGSRN) (Li et al., 2015): A dual-network system utilizing both SAR and optical images to enhance SAR resolution.

4. DC2SCN (Deep CNN with Skip Connection and Network in Network): A model designed specifically for SAR super-resolution, handling the real and imaginary parts of SAR data separately to preserve phase integrity.

Each model was trained using a combination of Sentinel-1, COSMO-SkyMed, and Sen1-2 dataset patches. The training process involved Z-score normalization, where pixel intensities were standardized to ensure optimal network convergence. The models were assessed using Peak Signal-to-Noise Ratio (PSNR) and Structural Similarity Index Measure (SSIM). As a baseline, we compared the deep learning models against bicubic interpolation, a commonly used upscaling method in image processing.

The experimental results, evaluated at a global scale using the Sen1-2 dataset, indicate significant improvements in SAR image resolution using deep learning techniques. The RRDB model outperformed the other architectures, achieving the highest PSNR and SSIM scores. The OGSRN model, which incorporates Sentinel-2 optical data, performed worse than RRDB despite its additional guidance input. This could be explained by variations in domain between SAR and optical images, which might cause feature extraction conflicts.

Overall, the results show that deep learning-based super-resolution can enhance SAR imagery quality significantly. Compared to bicubic interpolation, the best-performing model demonstrated an 18% PSNR increase (e.g., ~25 dB to ~29.5 dB) and a 2% SSIM improvement (e.g., 0.85 to 0.87), with RRDB outperforming OGSRN by 2-3 dB, highlighting SAR-only models' strengths. The visual result presented in Figure 4 (e.g., original vs. filtered COSMO-SkyMed patches) reinforced these findings, showing sharper edges and textures. This approach enhances SAR imagery for ground instability mapping in Gummern, aligning with S34I goals for extraction and closure phases of mining.

These findings underscore the potential of deep learning for SAR image enhancement and highlight future directions for improving model architecture and dataset quality.

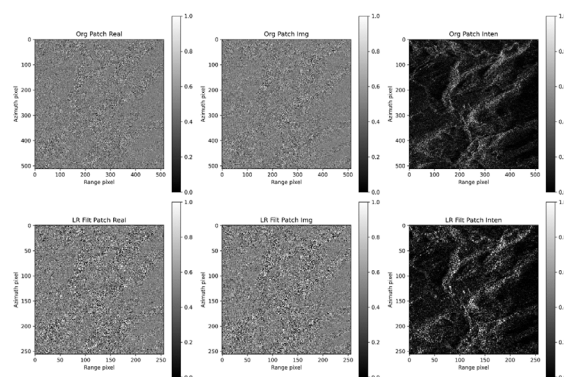


Figure 4: Original patch (first row) and filtered patch (second row) of COSMO-SkyMed sample.

5 UAV SURVEY

UAV Photogrammetry was used to perform several UAV surveys at the quarry with Phantom 4 Real Time Kinematic (RTK) + RGB camera. Because of variable terrain heights, terrain following method, i.e. flying at the same height above ground, proved to be the most efficient. The steepest part of the quarry was additionally surveyed with so-called angled flight mode. Ground Control Points (GCPs) were established for each survey and measured with RTK GNSS equipment to use later in image processing, ensuring better product accuracy. The latter are dense point clouds, 3D models, digital surface models (DSM), digital terrain models (DTM), and orthophotos. The flight height above ground was 100 m, resulting in a Ground Sampling Distance (GSD) of 3 cm.

Since multiple surveys were conducted, performing change detection for the same product across different dates is possible. One of the possibilities is monitoring deposited material in waste dumps by comparing two or more DEMs, which is especially useful in the northern part of the quarry at waste dumps. Figure 5 represents a calculated difference between DEMs, created from two different surveys.

High-resolution UAV data (especially DEM) served as a reference for less detailed remote sensing methods for terrain mapping, such as tri-stereo mapping, which is discussed in the Chapter 6.

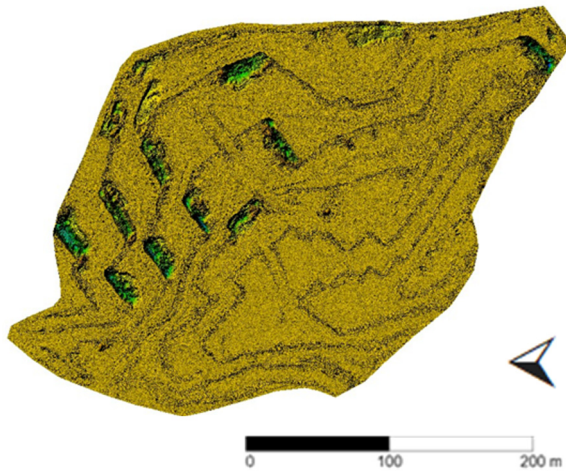


Figure 5: Differences between two DEMs produced from UAV.

6 TRI-STEREO MAPPING

Pléiades Neo tri-stereo consists of images that were collected during the same pass from different sensor-viewing angles (along-track stereo): forward (F), close to nadir (N) and backward (B). In the study, only panchromatic bands are used. Table 1 summarises the main acquisition parameters and characteristics of the images used.

Table 1: Acquisition parameters of the used Pléiades Neo tri-stereo images: incident angles (across-track, along-track and overall), GS), area, the computed [5] stereo intersection angles between two Pléiades scenes and their base-to-height ratio (B/H).

View	F	N	B
Across-track (°)	6.34	4.56	2.76
Along-track (°)	-7.67	-0.29	7.10
Overall (°)	9.90	4.57	7.61
GSD (m)	0.31 x 0.31	0.30 x 0.30	0.30 x 0.30
Area (km ²)	130.89	130.84	130.31
Convergence (°)	7.55 (FN)	7.60 (NB)	15.14 (FB)
B/H Ratio	0.13 (FN)	0.13 (NB)	0.27 (FB)

The initial orientation of the images was set using the Rational Function Model (RFM) containing 80 Rational Polynomial Coefficients (RPCs). RPCs allow the transformation between object and image space. Additionally, 25 tie points were automatically measured to improve the relative orientation of the images. GCPs, which were evenly distributed across the area, avoiding hilly and overgrown areas, were then measured on all tri-stereo images to improve

their georeferencing. Multiple rounds of bundle block adjustment were performed using different GCPs as checkpoints. The maximum difference in the individual coordinate components of the checkpoints was 31 cm. In the final block adjustment, we used all GCPs surveyed in the field. Final Root Mean Square Error (RMSE) was 0.35 on image level (given in pixels) and 0,21 m on GCPs (0.14 m in Easting, 0.15 m in Northing and 0.03 m in height). The dense image matching algorithms were applied to oriented images to extract surface points, from which the DEM with a spatial resolution of 0.5 m was interpolated. Figure 6 shows the terrain shaded relief of DEM produced from Pléiades Neo tri-stereo panchromatic images.

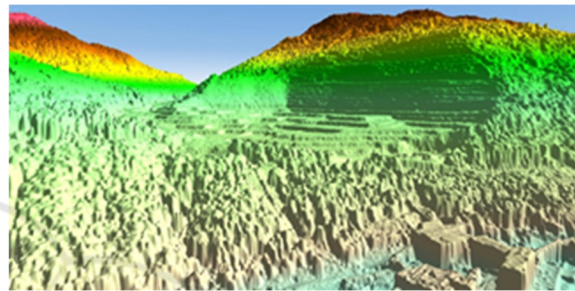


Figure 6: Terrain shaded relief of digital elevation model produced from tri-stereo imagery.

The accuracy of the produced DEM was estimated by comparing it to those produced with UAV surveys that were performed before and after the tri-stereo acquisition. 190 control points were extracted from UAV DEMs in the areas where no changes were detected between two consecutive surveys. Additionally, the satellite DEM was registered to those un-changed areas using Iterative Closest Point (ICP). The high accuracy of DEM, produced from satellite images was evaluated using the methodology proposed by EuroSDR (Höhle & Potuckova, 2011). We have achieved a mean value of 4.9 cm, RMSE of 30.1 cm, and standard deviation of 29.7 cm. Figure 7 shows the absolute distances between Pléiades Neo DEM and UAV DEM. The most extensive distances occur at the steep terraces in the quarry. The RMSE size is in the range of spatial resolution of the images and comparable to the results obtained by other authors (e.g. Loghin et al., 2020).

Pléiades Neo-derived DEM was additionally compared to DEM, created from WorldView-2 data. The latter captures images of the same area from different angles (stereo images). The slight displacement between the stereo pairs allows for depth perception and DEMs creation. The volume changes in the areas where waste dumping occurred are summarized in Figure 8.

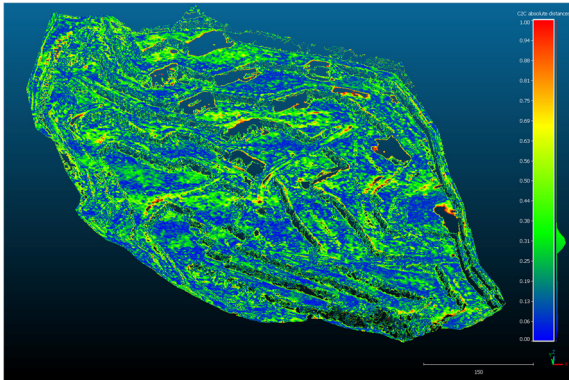


Figure 7: The absolute distances between Pléiades Neo DEM and UAV DEM after the registration.

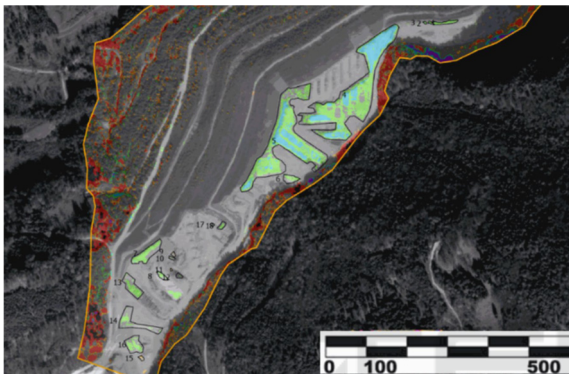


Figure 8: Volumes of waste dumps between Pléiades Neo-derived DEM and from WorldView-2 DEM.



Figure 9: LGMS installed in Gummern.

Geodetic monitoring of displacements started on 03.04.2023 and is still ongoing, with the LGMS operating continuously for almost two years. The open-source software RTKLIB (demo33_g) was used to post-process GNSS observations, with further details on the processing strategy provided in Table 2.

Table 2: Processing parameters used in RTKLIB.

Positioning mode	Static
Frequencies	L1+L2/E5b
Filter type	Forward
Cutt-off angle	10°
Sampling rate	10s
Iono/Troposphere correction	Broadcast/Sastamoinen
Satellite ephemeris	Broadcast
Satellite systems	GPS+GLO+Galileo
Ambiguity	Continuous (Lambda)
GNSS Antenna	AS-ANT2BCAL(igs14)

7 GNSS MONITORING

Low-Cost GNSS Monitoring Station (LGMS) was developed using low-cost GNSS receivers and antennas to continuously monitor displacement with high precision and decreased costs (Hamza et al., 2021, 2023). The main components of the LGMS are the ZED-F9P GNSS module and survey-calibrated antenna (AS-ANT2BCAL). The LGMS can work in remote areas without electricity connection since it uses solar panels to charge the battery from which the systems get the electricity (Figure 9). It acquires and stores GNSS observations continuously, which are later post-processed to estimate the daily displacement of the monitoring locations.

Four LGMS stations were deployed in Gummern, with two stations, F1 and F2 (Figure 10), installed on stable ground to be used as reference stations. These reference stations were used to estimate displacements at ST1 and ST2 (Figure 11 and Figure 12), which were positioned on the waste dump where displacements were expected.

The results indicated that in ST1 horizontal and vertical displacements of 20 and 40 mm occurred, respectively, while larger displacements of 40 mm horizontally and 70 mm vertically were noticed in ST2.



Figure 10: Locations of GNSS measuring stations.

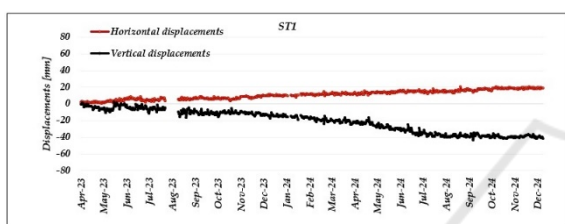


Figure 11: Horizontal and vertical displacement in ST1.

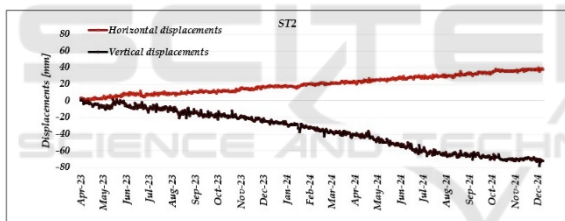


Figure 12: Horizontal and vertical displacement in ST2.

8 CONCLUSIONS

This work presents preliminary results of several EO methodologies designed to address specific needs in monitoring mining activities. We produced DEMs using photogrammetric data and satellite imagery, specifically from stereo and tri-stereo images. The results demonstrate that the quality of the DEM generated from satellite data is comparable to that of UAV-derived DEMs. Additionally, we found that both InSAR and low-cost GNSS data capture the same ground motion trends. While GNSS provides daily displacement measurements, which InSAR does not, InSAR offers a much denser result with broader spatial coverage. Furthermore, we showed that SAR imagery can enhance spatial resolution when processed with higher-resolution images.

By evaluating these methods, we provide decision makers with important information on the trade-offs between accuracy, spatial coverage and cost-effectiveness. The results emphasize the importance of a multi-sensor approach for comprehensive monitoring. However, further work is needed to validate these results. We are focusing on defining pipelines that will utilize the most effective methods and develop them into tools and services. This includes estimating the cost and value that the products will have for users so that operational services can be offered commercially.

ACKNOWLEDGEMENTS

This study is funded by the European Union under grant agreement no. 101091616 (<https://doi.org/10.3030/101091616>), project S34I – SECURE AND SUSTAINABLE SUPPLY OF RAW MATERIALS FOR EU INDUSTRY.

REFERENCES

- Berardino, P., Fornaro, G., Lanari, R., & Sansosti, E. (2002). A new algorithm for surface deformation monitoring based on small baseline differential SAR interferograms. *IEEE Transactions on Geoscience and Remote Sensing*, 40(11), 2375–2383. <https://doi.org/10.1109/TGRS.2002.803792>
- Falabella, F., Serio, C., Masiello, G., Zhao, Q., & Pepe, A. (2022). A Multigrid InSAR Technique for Joint Analyses at Single-Look and Multi-Look Scales. *IEEE Geoscience and Remote Sensing Letters*, 19. <https://doi.org/10.1109/LGRS.2021.3086271>
- Hamza, V., Stopar, B., Ambrožič, T., & Sterle, O. (2021). Performance Evaluation of Low-Cost Multi-Frequency GNSS Receivers and Antennas for Displacement Detection. *Applied Sciences*, 11(4), 6666. <https://doi.org/10.3390/app11146666>
- Hamza, V., Stopar, B., Sterle, O., & Pavlovčič-Prešeren, P. (2023). A Cost-Effective GNSS Solution for Continuous Monitoring of Landslides. *Remote Sensing*, 15(9), 2287. <https://doi.org/10.3390/rs15092287>
- Höhle, J. & Potuckova, M. (2011). Assessment of the Quality of Digital Terrain Models. European Spatial Data Research. https://www.eurosd.net/sites/default/files/uploaded_files/eurosd_publication_ndeg_60.pdf
- Li, Y., Zhou, L., Xu, F., & Chen, S. (2022). OGSRN: Optical-guided super-resolution network for SAR image. *Chinese Journal of Aeronautics*, 35(5), 204–219. <https://doi.org/10.1016/j.cja.2021.08.036>
- Loghini, A., Otepka-Schremmer, J., & Pfeifer, N. (2020). Potential of Pléiades and WorldView-3 Tri-Stereo DSMs to Represent Heights of Small Isolated Objects.

Sensors, 20(9), 2695. <https://doi.org/10.3390/s20092695>

Pepe, A., Solaro, G., Calò, F., & Dema, C. (2016). A minimum acceleration approach for the retrieval of multiplatform InSAR deformation time series. *IEEE Journal of Selected Topics in Applied Earth Observations and Remote Sensing*. 9(8), 3883–3898. <https://doi.org/10.1109/JSTARS.2016.2577878>

Ronneberger, O., Fischer, P., & Brox, T. (2015). *U-Net: Convolutional Networks for Biomedical Image Segmentation*. <https://doi.org/10.48550/arXiv.1505.04597>

Wang, X., Yu, K., Wu, S., Gu, J., Liu, Y., Dong, C., Loy, C. C., Qiao, Y., & Tang, X. (2018). *ESRGAN: Enhanced Super-Resolution Generative Adversarial Networks*. <http://arxiv.org/abs/1809.00219>

